Proceedings of the
International Conference on Mechanical Engineering 2003
(ICME2003) 26- 28 December 2003, Dhaka, Bangladesh

ICME03-FL-02

HYSTERESIS PHEOMENA APPEARING IN THE PERFORMANCE OF WELLS TURBINE

M. Mohammad[1], **Y. Kinoue**[1], **T. Setoguchi**[1], **K. Kaneko**[1] **and A.K.M.S. Islam**[2]

[1]Department of Mechanical Engineering, Saga University, 1, Honjo, Saga, 840-8502, Japan,
[2]Mechanical Engg. Dept., Bangladesh University of Engg. & Tech., Dhaka-1000, Bangladesh.

ABSTRACT

A Wells turbine for wave power conversion has hysteretic characteristics in a reciprocating flow. The numerical investigations were made by unsteady three-dimensional Navier-Stokes numerical simulations. The turbine characteristics show the counterclockwise hysteretic loop in the unstalled condition, which can be associated with a streamwise vortical flow appearing near the blade suction surface. In deep stall condition, the turbine characteristics show the clockwise hysteretic loop, which is similar to the dynamic stall of an airfoil.

Keywords: Wave power, Fluid machinery, Wells turbine.

1. INTRODUCTION

In the past two decades, worldwide efforts have been devoted to the development of energy conversion from ocean waves. One of the most applicable devices for wave energy is the combination of an Oscillating Water Column (OWC) as a primary converter and a self-rectifying air turbine as a secondary one (Fig.1).

The Wells turbine is one of the most suitable air turbine for energy conversion from oscillating air flow. Usually, the unsteady characteristics of Wells turbine are predicted by computer simulation on the basis of the steady characteristics [1]. It seems to be reasonable to employ such a quasi-steady analysis because the nondimensional wave frequency (based on the relative velocity and the blade chord length) is the order of 10^{-4}. However, it results in inaccurate predictions of the performance, since the Wells turbine has hysteretic characteristics in an unsteady flow [2 - 4].

Dynamic stall of an airfoil is well-known as an unsteady aerodynamic phenomenon which has hysteretic characteristics, and a lot of researchers have reported many kinds of aspects of dynamic stall of an airfoil [5 - 8]. But the hysteretic loop of the lift-attack angle characteristics of the dynamic stall is counterclockwise and opposite to the clockwise one of the Wells turbine in unstalled condition. So the mechanism of the hysteretic characteristics of Wells turbine should be clarified for the better design of the system for wave power conversion.

In order to investigate the hysteretic behavior of Wells turbine, unsteady, 3 dimensional Navier-Stokes numerical simulations were conducted for the flow field around a blade of the Wells turbine.

2. NUMERICAL ANALYSIS

Numerical simulations in this paper were made in the Wells turbine of which the hysteretic behavior was investigated experimentally by Inoue et al. [2]. Summaries of the experiments are briefly mentioned. The test rig consists of a 1.4 m diameter cylinder with a piston disk, a rectangular settling chamber, and a 0.3 m diameter test section with a bell mouth entry and a diffuser exit. The turbine rotor is placed at the center of the test section, and can be operated at arbitrary rotating speed. A sinusoidal axial air flow is produced by controlling the motion of the piston (0.167 Hz of frequency in this paper). The unsteady turbine performances were examined in one-half period of the sinusoidal change in axial flow velocity. Experimental results of the half part of the full cyclic hysteretic characteristics by Alcorn and Beattie [4] reveal almost similar to the one by Inoue et al. [2]. Table 1 shows the specifications of the turbine rotor used in this study. Model testing was made in such the way that the turbine rotating speed were set at zero axial flow velocity condition once, then the turbine output torque T, the air flow Q and the total pressure drop across the rotor ΔP_0 were measured by keeping the turbine speed constant. The Reynolds number based on the blade chord length and relative velocity at mean radius is about 2.4×10^5.

A commercial code, FLUENT 5, was used for the numerical analysis. The unsteady 3-dimensional and filtered Navier-Stokes equations were discretized by the finite volume method. The rotating frame fixed to turbine rotor was adopted. The second order accuracy upwind differencing scheme was used for the convection term and the second order accuracy implicit method was used for the time discretization. The RNG-SGS model [9], which

is one of LES model, was used to calculate the subgrid-scale turbulent viscosity. The unsteady calculations were made in one-half period of the sinusoidal change in an axial flow velocity.

The computational domain was extended 4 and 8 blade chord lengths upstream and downstream of the blade, respectively, as shown in Fig.2. Fig.3 shows the perspective view of grids. The structured, hexahedral grids of O-type were used around the blade, while H-type grids were used for the upstream and downstream regions. The total numbers of the grids are approximately 560,000. 3 grids were embedded in the region of tip clearance. The calculation for finer grids (approximately 703,000 grids, 6 grids for tip clearance) was made to check the grid dependency of the calculation for the objective (560,000) grids.

The non-slip boundary conditions were used for the hub surface, the pressure and suction side of the rotor surfaces. The moving casing wall was used because of the rotating frame of reference. The periodic boundary conditions were used for the surfaces of circumferential sides. On the upstream boundary, the inlet velocities were given at each time step, where the axial velocities were given from the flowrate and the circumferential velocities were given from the rotor rotating speed. On the downstream boundary, the static pressures were set at each time step. The results of the steady flow calculation for attack angle α_R=0° were used as the initial condition, which corresponded to the experimental condition. The nondimensional distance of the first grid point from the blade surface was less than 5.0 based on the friction velocity and the kinematic viscosity of air.

3. RESULTS IN UNSTALLED CONDITION

Figure 4 shows the experimental [2] and calculated results of hysteretic behaviors of the total pressure coefficient C_A against the attack angle α_R in one-half period of the sinusoidal flow. These coefficients are defined as follows.

$$C_A = \Delta P_0 Q / \left(\rho \left(v_a^2 + U_R^2 \right) z b l v_a / 2 \right) \quad (1)$$

$$\alpha_R = \tan^{-1}\left(v_a / U_R \right) = \tan^{-1} \phi \quad (2)$$

where ΔP_0 denotes the total pressure drop across the rotor, Q air flow rate, ρ density of air, v_a axial velocity, U_R circumferential velocity at mid span, z number of blades, b span of the blade, T torque of the rotor, r_R radius at mid span, α_R attack angle and ϕ flow coefficient.

The attack angle varies between 0° and its maximum value in phase with the oscillating flow. In the course of the cycle the experimental C_A value (broken line) during acceleration of axial velocity (increasing α_R), is lower than that during deceleration (decreasing α_R), and then an counterclockwise hysteretic loop appears as shown in Fig.4. If the hysteretic behavior was caused by the dynamic stall of blade, a clockwise hysteretic loop would be seen [5-8]. Therefore, the mechanism of hysteretic behavior of Wells turbine should be different from the mechanism of the dynamic stall in unstalled condition.

As for the agreement of the calculated values with the experimental data in Fig.4, qualitative agreements are well obtained, although the calculated values are a little smaller than the experimental data. Maximum values of the calculated results of C_A agree well with the experiment quantitatively. As for the grid dependency of C_A, C_A values for finer grids are a little (0.1 of C_A in the maximum case) larger than the values for the objective grids in the accelerating flow, but the maximum C_A value and the C_A values in the decelerating flow for finer grids is almost the same as the C_A values for the objective grids. The calculation of the objective grids can qualitatively simulate the hysteretic phenomenon of the Wells turbine in spite of comparably small numbers of grid points in the tip clearance. In the following description, the mechanism of the hysteretic characteristics of the Wells turbine is considered through the examination of the calculated flow fields.

Figure 5 shows the streamlines near the suction surface starting from the leading edge of the blade. For α_R =6°, the flow near the hub surface separates more upstream than the flow near the tip side in the accelerating flow. This region of separation cannot be seen for α_R =6° in the decelerating flow. In addition, some of the streamlines near the trailing edge go away from the suction surface in the tip side region, due to the effect of the tip leakage flow. For α_R =12°, the separation region is extended in both accelerating and decelerating flows. The separation region in the accelerating flow becomes more enlarged than the one in the decelerating flow.

Figure 6 shows the streamlines starting from the trailing edge of the blade. The streamlines crossing over the blade suction surface come from the trailing edge of the left side blade. A clockwise vortex exists near the hub, which is caused by the strong downward flow near the trailing edge. The clearest vortex can be seen in the accelerating flow for α_R =6° among the four cases in Fig.6.

4. HYSTERESIS IN UNSTALLED CONDITION

Figure 7 shows an illustration of the flow structure obtained by the present numerical simulation in unstalled condition. At high angles of attack a separation vortex (2) appears on the blade suction surface in the hub side to reduce the blade circulation, because of the excessive angle of attack near the hub. A strong downward flow (3) is induced by the separation vortex near the trailing edge. It brings about the clockwise vortical wake flow (4a), which affects to enlarge the flow separation on the adjacent blade suction surface (4b). The intensity of the vortical flow varies in the accelerating and the decelerating flow process for the following reason.

In the accelerating flow process, as the blade circulation increases, vortices opposite to the blade circulation is shed from the trailing edge according to Kelvin's theorem. The stronger vortices are shed at a larger radius because the blade circulation increases more than at a smaller radius. Then, the clockwise trailing vortices are generated according to Helmholtz's theorem. Therefore, the clockwise vortical flow is intensified by these vortices. In the decelerating flow process where the blade circulation decreases, the shed vortices are in the same direction of the blade circulation.

They form counterclockwise trailing vortices, which suppress the vortical wake flow. Since the stronger

Blade profile	NACA0020
Number of blades z	6
Blade chord length l	90 mm
Solidity at tip σ_t	0.57
Aspect ratio AR	0.5
Tip radius R_t	149 mm
Tip clearance TC	1 mm
Setting angle γ	0°

Table 1 Turbine models

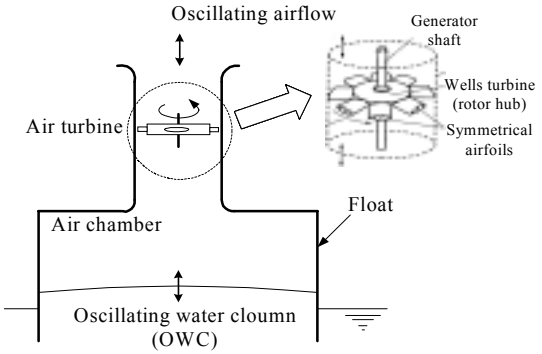

Fig.1 Schematic view for OWC device

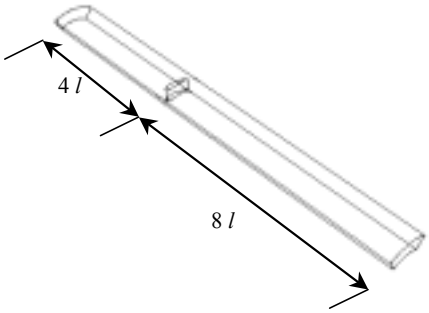

Fig.2 Computational domain

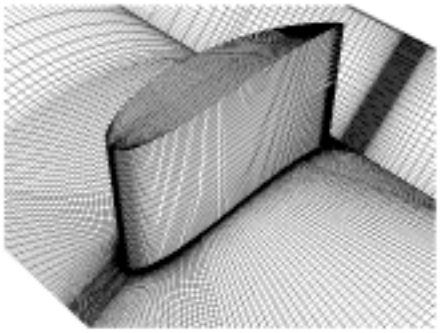

Fig.3 Perspective view of grids

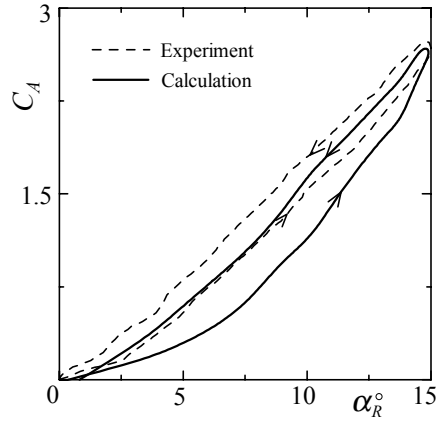

Fig.4 Total pressure coefficient

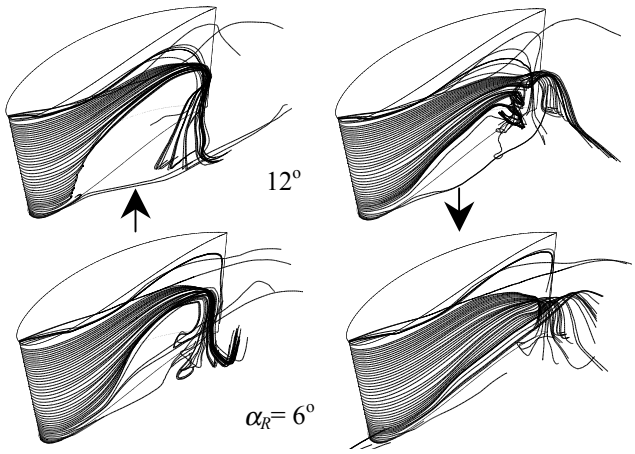

Accelerating flow Decelerating flow

Fig.5 Streamlines near the suction surface

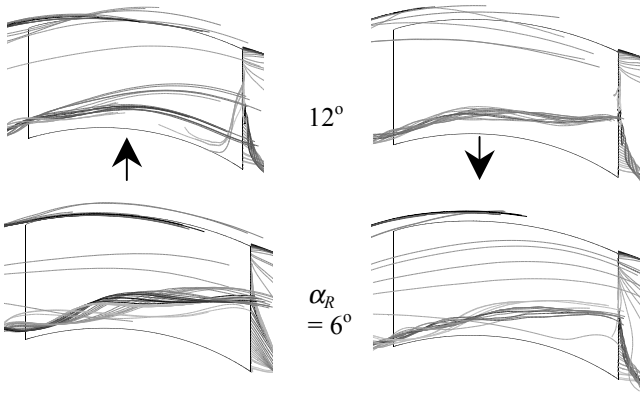

Accelerating flow Decelerating flow

Fig.6 Streamlines starting from the trailing edge

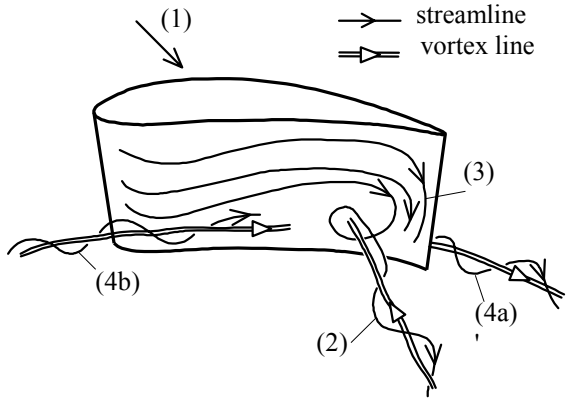

(1):incoming flow, (2):separation vortex flowing downstream, (3):downward flow to make a vortical wake flow, (4a):vortical wake flow affecting the adjacent blade, (4b):vortical wake flow to enlarge the flow separation

Fig.7 Illustrations of the flow structure in blade suction side

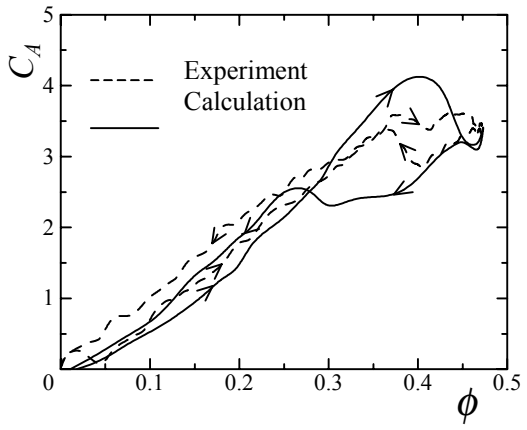

Fig. 8 Total pressure coefficient including deep stall

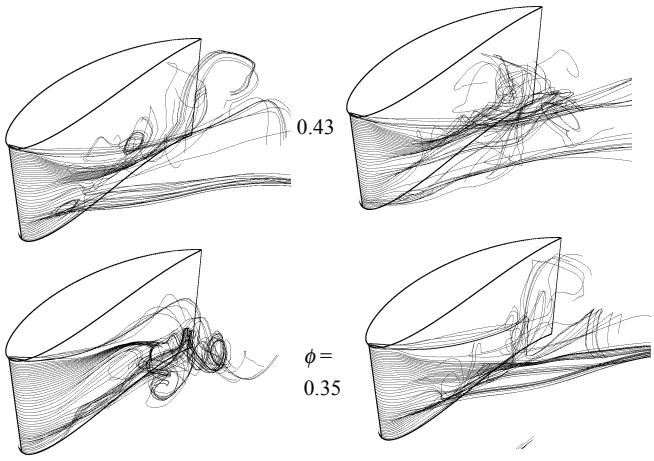

Accelerating flow Decelerating flow

Fig. 9 Streamlines near the blade suction surface in deep stall condition

vortical wake flow enlarges the separation on the suction surface of the adjacent blade, the performance in the accelerating flow process becomes lower than in the decelerating flow process in unstalled condition.

5. RESULTS IN DEEP STALL CONDITION

Figure 8 shows the experimental and calculated results of hysteretic behaviors of C_A for ϕ_{max} =0.47, the solid and broken lines show the calculation and the experiment, respectively. As shown in Fig. 8, Calculated results of C_A have the counterclockwise hysteretic loop in the unstalled condition and the clockwise hysteretic loop in deep stall condition, although the agreements of the calculated values with experimental data are not good.

Figure 9 shows the streamlines near the suction surface starting from the leading edge of the blades. In the unstalled condition, the flow near the hub surface separates more upstream than the flow near the tip side in the accelerating flow. For ϕ=0.35 and 0.43 in deep stall condition, however, the large flow separations can be seen around the tip regions besides the separation near the hub.

6. CONCLUSUIONS

In order to elucidate the hysteretic characteristics of Wells turbine, unsteady, 3-dimensional Navier-Stokes numerical simulations were conducted using the commercial code of FLUENT5 for the case of an axial velocity changing sinusoidally. Conclusions are summerized as follows.

(1) The cause of hysteretic behavior in unstalled condition is associated with this clockwise vortex. In the accelerating flow, the intensive existence of the clockwise vortex extends the separation region on the blade suction surface toward the mid span region, which leads to the reduction of the torque coefficient and the total pressure coefficient. In the decelerating flow, the separation region is reduced as the vortex is weakened.

(2) The calculated results using RNG-SGS model can follow the experimental results of both the counter clockwise loop in the unstalled condition and the clockwise loop in deep stall condition. In the condition without stall, the flow separation can be seen only near the hub, while the flow separation can be seen both near the hub and near the tip in deep stall condition.

7. REFERENCES

1. Inoue, M., Kaneko, K., Setoguchi, T. and Simamoto, K., 1985, "Studies on Wells Turbine for Wave Power Generator (4th Report, Starting and Running Characteristics in Periodically Oscillating Flow)," Trans. JSME(B), 51-468, pp.2746-2751(in Japanese).
2. Inoue, M., Kaneko, K., Setoguchi, T. and Koura, F., 1987, "Hysteretic Characteristics of Wells Turbine in Reciprocating Flow," Trans. JSME(B), 53-496, pp.3699-3704(in Japanese).
3. Setoguchi, T., Kaneko, K., Hamakawa, H and Inoue, M., 1990, "Measurement of Hysteresis on Wells Turbine Characteristics in Reciprocating Flow," Proc. 1st International Symposium on Experimental and Computational Aerothermo-Dynamics of

Internal Flows, pp.537-543.
4. Alcorn, R.G. and Beattie, W.C., 1998, “Observations of Time domain Data on Wells Turbine in the Islay Wave-Power Plant,” Proc. 8th International Offshore and Polar Engineering Conference, 1, pp.81-85.
5. Ericsson, L.E. and Reding, J.P., 1987, “Fluid Dynamics of Unsteady Separated Flow, Part II. Lifting Surfaces,” Progress in Aerospace Science, 24, pp.249-356.
6. Shida, Y., Kuwahara, K., Ono, K. and Takami H., 1987, "Computation of Dynamic Stall of a NACA-0012 Airfoil," AIAA J., 25(3), pp.408-413.
7. Carr, L. W., 1988, "Progress in Analysis and Prediction of Dynamic Stall," J. Aircraft, 25(1), pp.6-17.
8. Leishman, J. G., 1990, "Dynamic Stall Experiments on the NACA 23012 Aerofoil," Experiments in Fluids, 9, pp.49-58.
9. Yakhot, V. and Orszag, S.A., 1986, “Renormalization Group Analysis of Turbulence (I. Basic Theory),” J. of Sci. Comp., 1(1), pp.3-51.

8. NOMENCLATURE

Symbol	Meaning	Unit
b	span of the blade	(m)
C_A	total pressure coefficient	(-)
l	chord length	(m)
r	radius	(m)
T	torque generated by rotor	(Nm)
U	circumferential velocity	m/s
v_a	axial velocity	m/s
x	distance from leading edge	(m)
z	number of blades	(-)
α	angle of attack	degree
ΔP_0	total pressure drop	(Pa)
ρ	density of air	kg/m^3
ϕ	flow coefficient	(-)